Conf-930405--42

UCRL-JC-113778
PREPRINT

OBSERVATION OF X-RAY ABSORPTION MAGNETIC CIRCULAR DICHROISM IN WELL-CHARACTERIZED IRON-COBALT-PLATINUM MULTILAYERS

A.F. JANKOWSKI
G.D. WADDILL
J.G. TOBIN

This paper was prepared for submittal to the
Materials Research Society
San Francisco, CA
April 12-16, 1993

April 1993

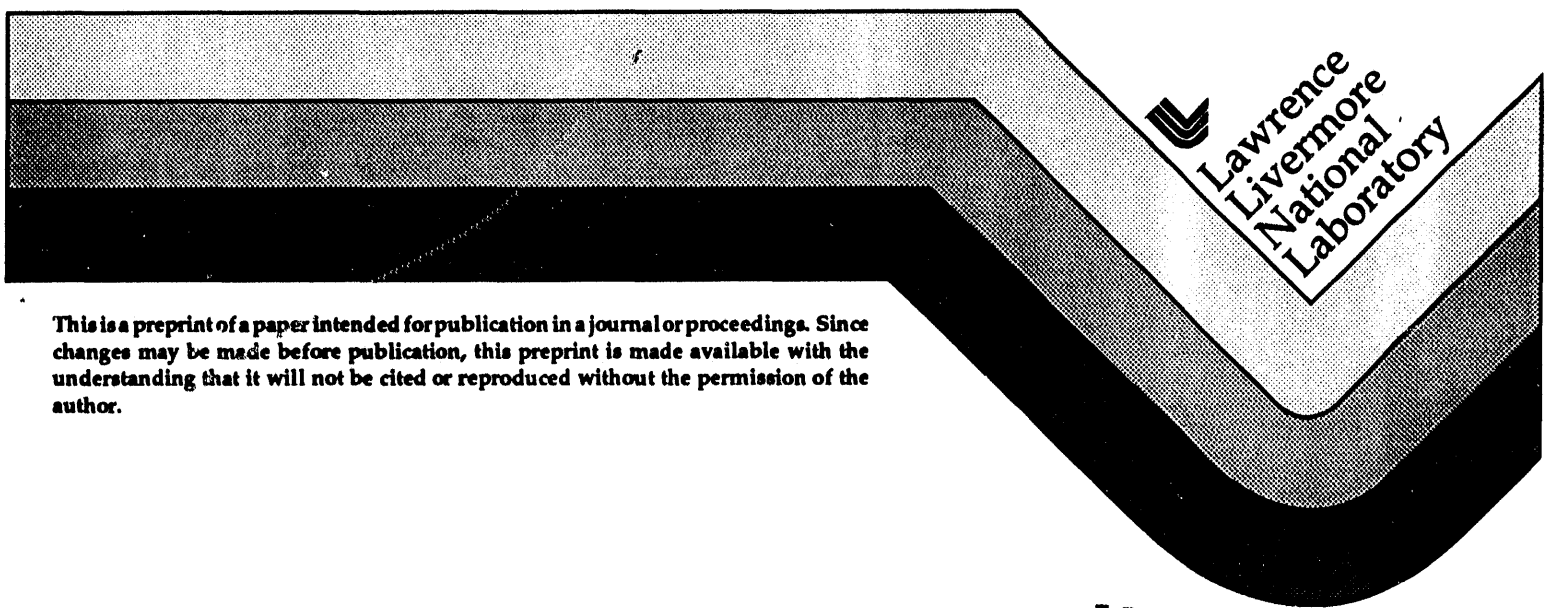

OBSERVATION OF X-RAY ABSORPTION MAGNETIC CIRCULAR DICHROISM IN WELL-CHARACTERIZED IRON-COBALT-PLATINUM MULTILAYERS

A.F. JANKOWSKI, G.D. WADDILL and J.G. TOBIN

Lawrence Livermore National Laboratory, Chemistry & Materials Science Department, P.O. Box 808, Livermore, California 94550 U.S.A.

ABSTRACT

Magnetic circular dichroism in the Fe 2p x-ray absorption is observed in multilayers of (Fe9.5Å/Pt9.5Å)$_{92}$. The magnetization and helicity are both in the plane of this multilayer which is prepared by magnetron sputter deposition. This sample is part of a study to examine magnetization in the ternary multilayer system of FeCo/Pt. Lattice and layer pair spacings are measured using x-ray scattering. The atomic concentration profiles of the multilayer films are characterized using Auger electron spectroscopy coupled with depth profiling. Conventional and high resolution transmission electron microscopy are used to examine the thin film, growth morphology and atomic structure.

INTRODUCTION

The observation of perpendicular magnetic anisotropy in the Co/Pt[1-4] and Fe/Pt[5] multilayer systems proves to be of interest for magnetic recording applications. The magnetic properties of Fe/Pt multilayer films are strongly dependent on the relative as well as absolute layer thicknesses.[6] X-ray absorption spectroscopy (XAS) is used for elemental analysis and magnetic circular dichroism (MCD) measurements. It is shown that MCD can be a useful technique for monitoring changes in the orientation of sample magnetization.[7] An in-plane magnetization of a (Fe9.5Å/Pt9.5Å)$_{92}$ multilayer thin film is found using both MCD and conventional magnetometry.[8] The MCD technique has the potential to follow the magnetic axis orientation in FeCo/Pt magnetic thin films as well as provide elemental specific determination of the magnetic moment.

SAMPLE PREPARATION

The FeCo/Pt multilayer samples are prepared using magnetron sputter deposition. The deposition chamber is cryogenically pumped to a base pressure of 1.3×10^{-5} Pa. A circular array of magnetron sources is situated 20 cm beneath an oxygen-free copper platen. The magnetron sources are operated in the dc mode at a 330-390 Volt discharge. An argon working gas pressure of 0.40 Pa is used at a flow rate of 15.5 cc min^{-1}. The substrates are sequentially rotated over each source at 1.0 rev min^{-1}. The target materials are >0.9994 pure. The polished Si substrates are cleaned with a procedure consisting of a detergent wash,

deionized water rinse, alcohol rinse and a N_2 gas drying prior to deposition. The substrates remain at a temperature between 293 and 306 K during the deposition. The sputter deposition rates, between 0.02 and 0.50 nm sec^{-1}, are monitored using calibrated quartz crystals. The quartz crystals indicate the component layer thicknesses (Sample column of Table I) and the layer pair thicknesses, $d_{FeCo/Pt}^{XTC}$. The multilayer films are grown to a 0.2μm thickness.

CHARACTERIZATION METHODS AND RESULTS

X-Ray Diffraction

The lattice and layer pair spacings of the FeCo/Pt multilayers are measured using x-ray diffraction. A powder diffractometer equipped with a graphite monochromator is operated in the θ/2θ mode at both grazing incidence and high angle using Cu $K\alpha$ radiation. The grazing incidence scans of the multilayer films (XRD column of Figs.1a-f) reveal the satellite reflections about (000) attributable to the composition modulation in the multilayer growth direction. The first three satellite peak positions (n = 1,2,3) are corrected for refraction and fitted to compute a layer pair spacing $d_{FeCo/Pt}^{XRD}$ (Table I). The layer pair spacings $d_{FeCo/Pt}^{XRD}$ are in agreement to within 0.01nm of the crystal monitor values $d_{FeCo/Pt}^{XTC}$. The high angle Bragg reflections indicate that the thin film samples are all oriented along the [111] direction of a face-centered-cubic (fcc) lattice. The interplanar spacing, $d_{(111)}^{XRD}$ (Table I), is generally intermediate to the values of pure Pt(111) at 0.2266nm and γFe(111) at 0.2106nm. A first-order satellite reflection below the Bragg reflection in the θ/2θ scans indicates layer pair spacings, from the relationship $[s_{(111)}-s_{satellite}]^{-1}$ where $s = d^{-1}$, for the films consistent with the grazing incidence measurements.[6]

Table I. Layer Pair and Interplanar Spacings (nm) of FeCo/Pt(111) Multilayers

Sample	$d_{(111)}^{XRD}$	$d_{FeCo/Pt}^{XRD}$	$d_{FeCo/Pt}^{XTC}$
$(Co3.9Å/Pt9.1Å)_{135}$	0.2223	1.295	1.294
$(Fe1.7ÅCo1.8Å/Pt9.7Å)_{135}$	0.2246	1.288	1.313
$(Fe9.5Å/Pt9.5Å)_{92}$	0.2193	2.008	1.895
$(Fe3.0Å/Pt9.7Å)_{135}$	0.2252	1.280	1.267
$(Fe3.1Å/Pt19.4Å)_{76}$	0.2270	2.228	2.245
$(Fe3.1Å/Pt38.8Å)_{44}$	0.2274	4.238	4.187

Auger Electron Spectroscopy

Atomic concentration profiles of the multilayer thin films are measured using Auger electron spectroscopy (AES) coupled with depth profiling. A 3 keV, 10 μA electron beam is used to generate the Auger electrons. The measured intensities of the 1.967 keV platinum peak (Pt MNN), the 703 eV iron peak (Fe LMM), the 272 eV carbon peak (C KLL) and the 503 eV oxygen peak (O KLL) from data accumulated in the derivative mode are used to compute the

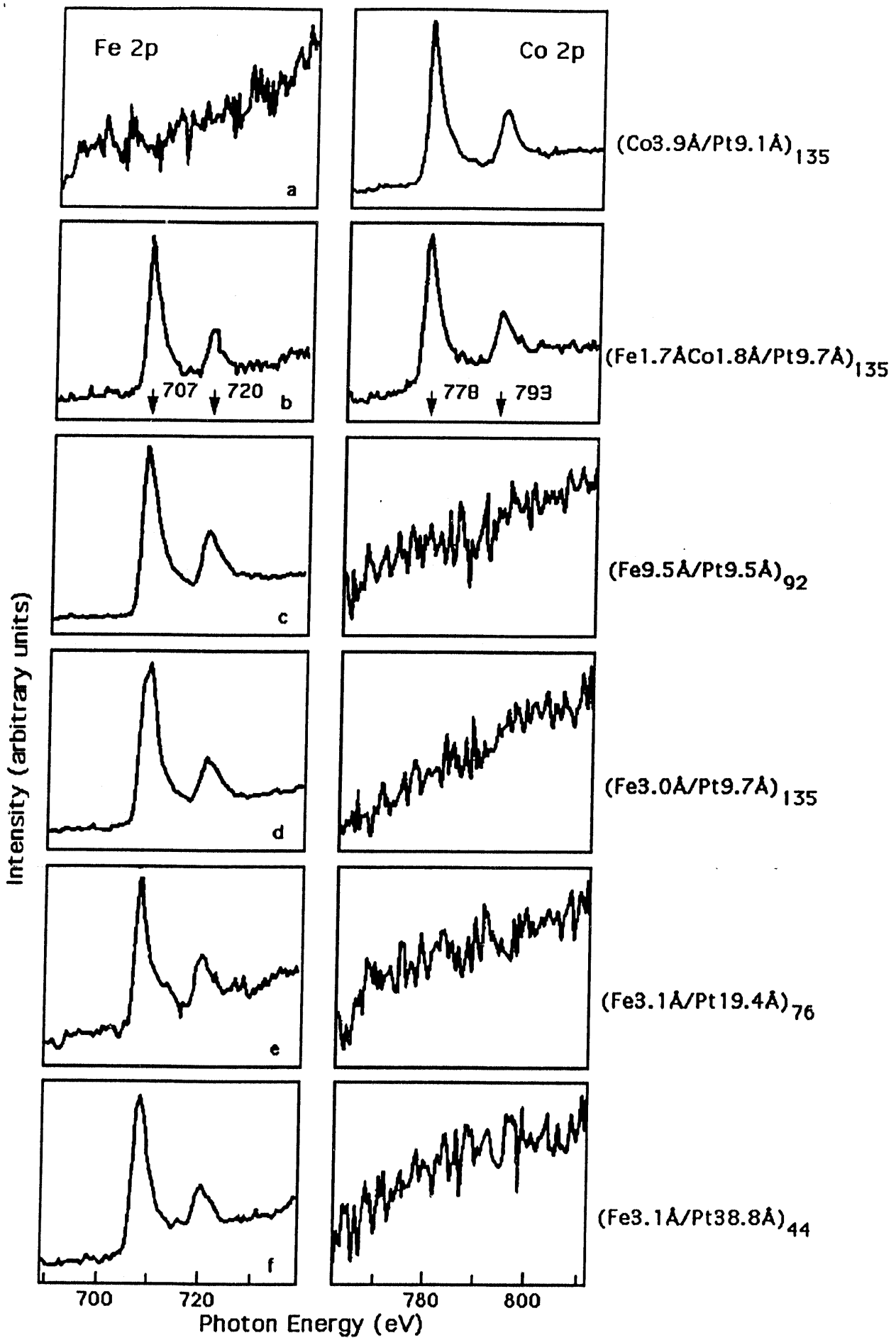

Figure 1. The columns correspond to the x-ray absorption at the Fe 2p and Co 2p edges using linear polarization and normal incidence measurement of the FeCo/Pt multilayer samples.

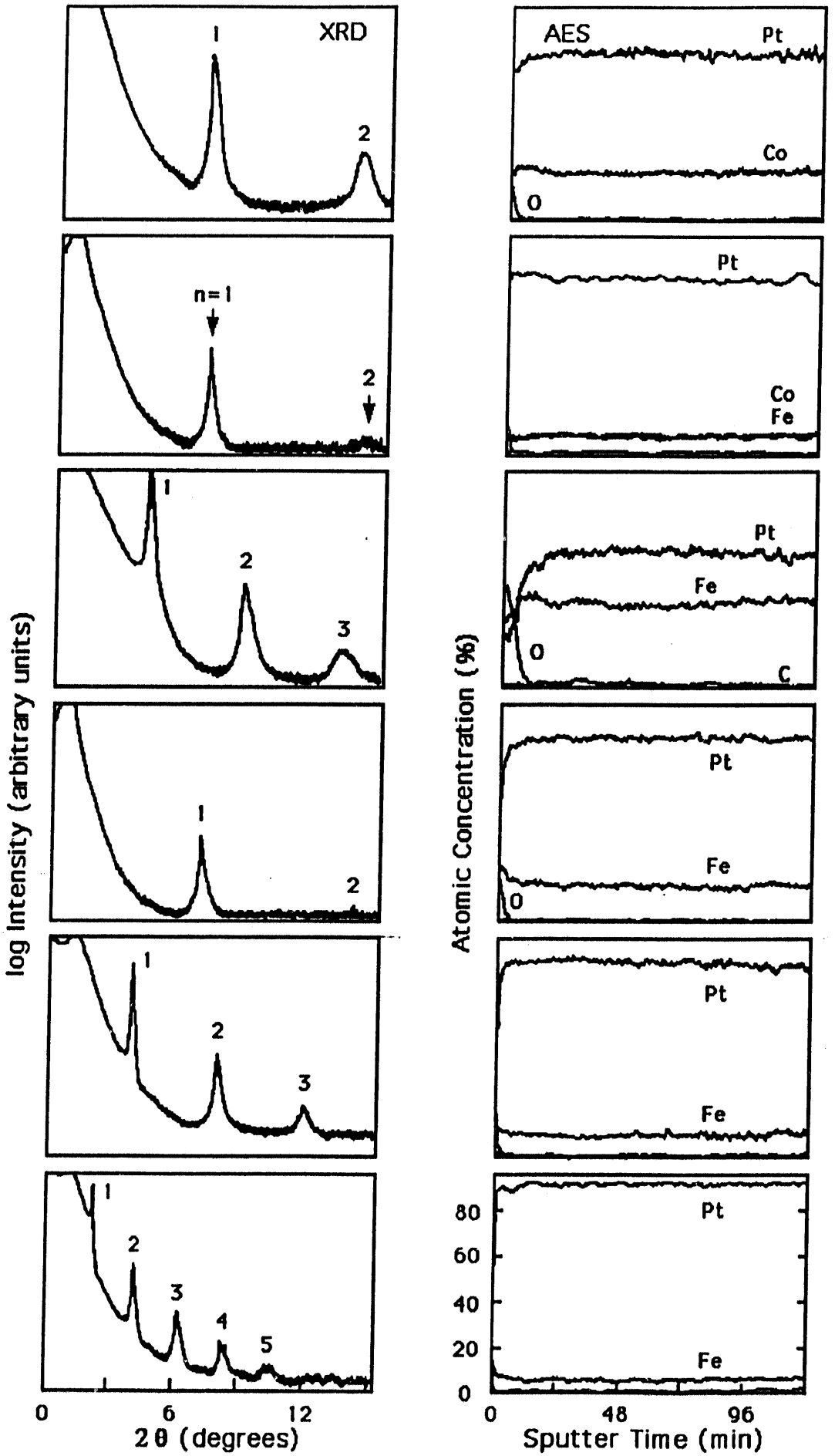

Figure 1.(continued) The columns correspond with grazing incidence x-ray diffraction (XRD) scans and Auger (AES) depth profiles of the FeCo/Pt multilayer samples, as listed in (a-f).

atomic concentrations. A 2 keV, 0.92 μA argon ion beam is used to sputter etch a 25 mm^2 area of the sample surface. The gas pressure for the sputter etch is $4x10^{-3}$ Pa whereas the Auger system base pressure is $6.7x10^{-8}$ Pa. Once the surface oxide is sputtered through, the film composition is shown to be uniform and free of any C or O contamination (AES column of Figs.1a-f). The concentration analysis of the films using AES are in agreement to within 10% of the absolute concentration value for each component as determined from the calibrated quartz crystal monitor readings of component layer thicknesses.

Transmission Electron Microscopy

Transmission electron microscopy (TEM) and high resolution imaging reveal the multilayer film morphology and lattice structure. The FeCo/Pt films, as imaged in both plan view (Fig.2a) and cross-section (Fig.2c), are typified by a dense columnar growth. The plan view electron diffraction patterns reveal the polycrystalline, in-plane nature of the films. The ring pattern (Fig. 2b) of this fcc phase is indexed to a lattice parameter of 0.3848nm. This lattice spacing corresponds quite well with the high angle diffraction data that gives a lattice parameter of 0.3798nm. Diffraction patterns, taken from the multilayer as viewed in cross-section, reveal a 5-8° mosaic of the lattice planes perpendicular to the [111] growth direction. Selected area diffraction patterns of individual grains, viewed in cross-section (Fig. 2d), clearly show the [111] growth direction of an fcc phase in this [110] pole projection. The FeCo/Pt thin film samples are therefore [111] textured in the growth direction but randomly oriented in-plane. The average grain size is 27-30nm, as measured from the bright field images (as Fig.2a). Lattice images, recorded at the Scherzer defocus condition using a 400 keV electron beam, show each grain to consist of a single-phase fcc structure (Fig.3).

X-ray Absorption Spectroscopy and Magnetic Circular Dichroism

The XAS and MCD measurements are performed on a spherical grating monochromator with the ability to generate soft x-rays with a high degree of linear or circular polarization.[9,10] The absorption measurements are made in a partial electron yield mode with a kinetic energy window centered around 50 eV. The XAS spectra (Fe 2p and Co 2p columns in Fig. 1a-f) are for normal incidence (i.e. 0° from the sample normal). The curves correspond to linear polarization scans for elemental analysis. The presence of Fe as well as Co is detected for even the smallest film concentrations, e.g. 7at.% Fe in sample $(Fe3.1Å/Pt38.8Å)_{44}$. For the MCD measurements, the samples are magnetized in-situ with a pulse coil capable of generating a 3kOe field. MCD in x-ray absorption is observed as a circular polarization dependent intensity variation in the L_2 and L_3 edges for 3d transition metals. The polarization dependence requires that the incident x-ray helicity (either parallel or anti-parallel to the direction of propagation) be aligned or anti-aligned with the sample magnetization.[7,11] The polarization dependence vanishes when these vectors are perpendicular. An intensity difference for the L_2 and L_3 white lines is apparent for sample $(Fe9.5Å/Pt9.5Å)_{92}$ demonstrating a remnant, in-plane magnetization of the film (Fig.4).

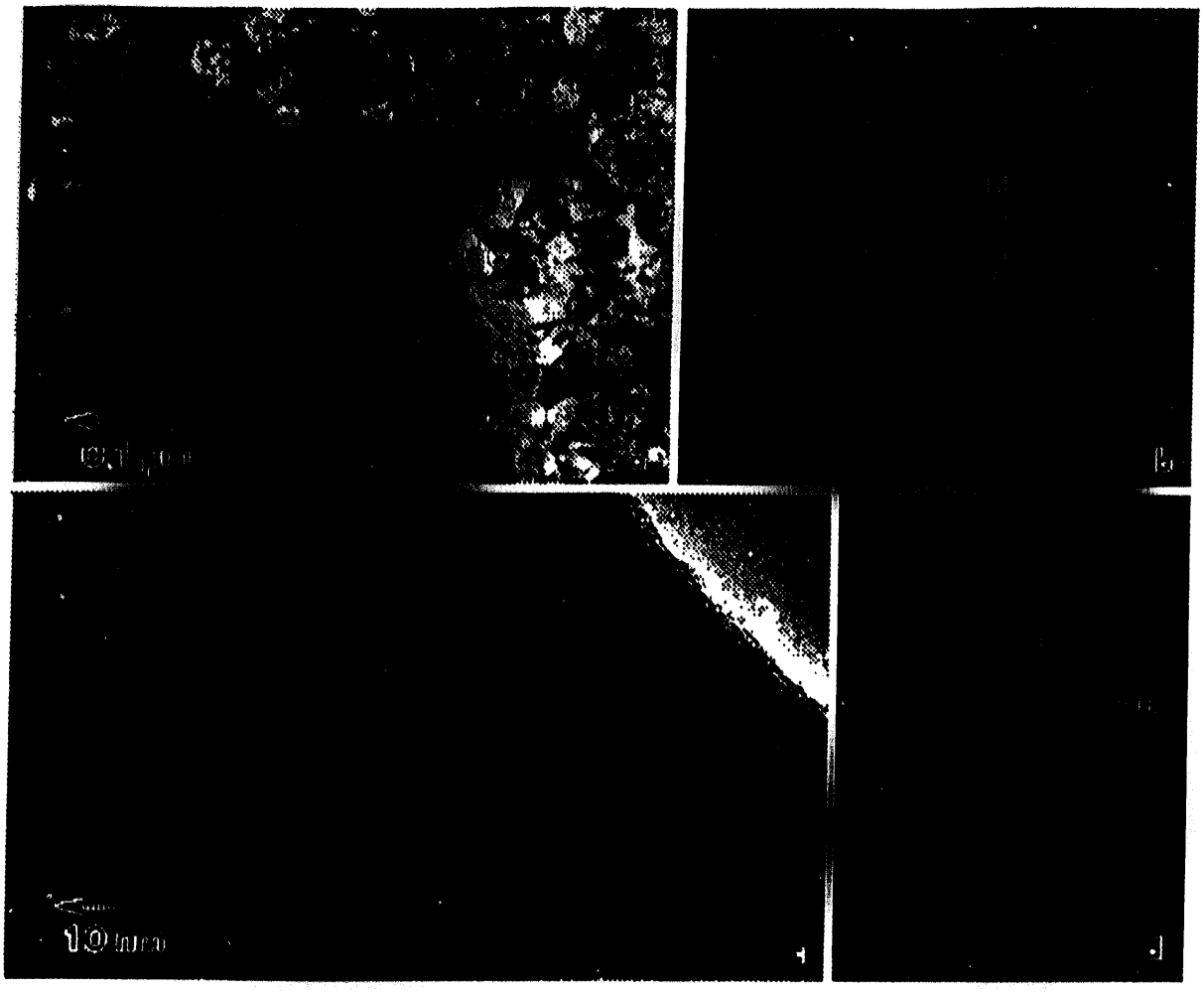

Figure 2. Conventional transmission electron microscopy of sample $(Fe9.5Å/Pt9.5Å)_{92}$, as imaged in plan view, reveals (a) the fine grain size in the bright field image and (b) the preferred (111) texture in the electron diffraction pattern of the film. Imaging of sample $(Co3.9Å/Pt9.1Å)_{135}$, as prepared in cross-section, reveals (c) layering perpendicular to the growth direction (indicated with an arrow) and (d) a [111] oriented, single-phase structure as seen in the [110] pole projection of this face-centered cubic, selected area diffraction pattern.

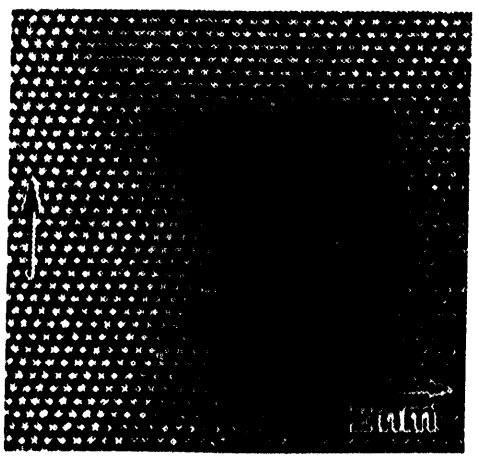

Figure 3. High resolution electron micrograph of the sample $(Fe9.5Å/Pt9.5Å)_{92}$, as imaged in cross-section. The growth direction is indicated with an arrow.

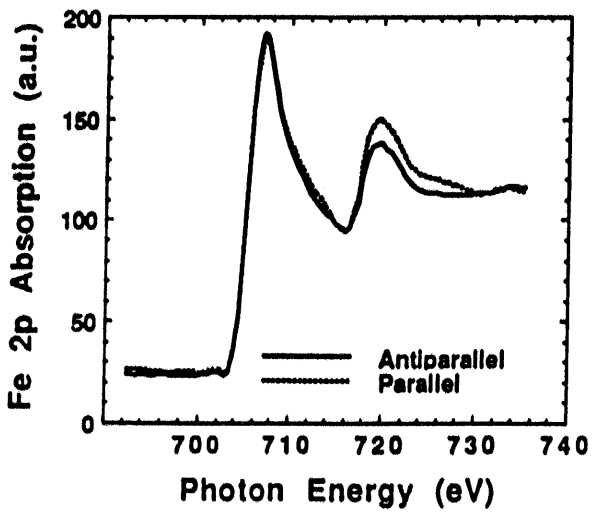

Figure 4. Fe L-edge absorption spectra of the $(Fe9.5Å/Pt9.5Å)_{92}$ multilayer for the x-ray helicity and majority d-electron spin nearly parallel (---) and antiparallel (—). This is an illustration of magnetic circular dichroism using circularly polarized x-rays.

DISCUSSION & SUMMARY

The relative strengths of the L_2 and L_3 absorption edges contain information about the spin-dependent density of states near the Fermi level and the spin-orbit splitting in the d-bands. Therefore, information is available about the spin and orbital magnetic moments of the material.[7,12-14] The spin moment analysis[7] applied to sample $(Fe9.5Å/Pt9.5Å)_{92}$ yields a value of $1 \pm 0.5\ \mu_B$/Fe. The analysis is complicated, however, by the polycrystalline surface. If the sample is not of a single domain, then MCD will average the domains yielding a moment that reflects the average projection of magnetization along the photon propagation direction.

In summary, we have studied the microstructure of FeCo/Pt multilayer films using x-ray diffraction and transmission electron microscopy, the composition using x-ray absorption and Auger spectroscopy, and the magnetic behavior using MCD. The correlation of structural properties with magnetic anisotropy requires detailed and elemental sensitive characterization. MCD enables the study of multi-element films, as FeCo/Pt, where the local moments can be determined for each component material.

ACKNOWLEDGMENTS

The MCD measurements were performed at the Stanford Synchrotron Radiation Laboratory. We thank Mark Wall for the transmission electron microscopy images. This work was performed under the auspices of the United States Department of Energy by Lawrence Livermore National Laboratory under contract W-7405-Eng-48.

REFERENCES

1 P.F. Carcia, A.D. Meinhaldt and A. Suna, Appl. Phys. **47**, 178 (1985).

2 P.F. Carcia, J. Appl. Phys. **63**, 5066 (1988).

3 Z. Zhang, P.E. Wigen and S.S.P. Parkin, J. Appl. Phys. **69**, 5649 (1991).

4 B.D. Hermsmeier, R.F.C. Farrow, C.H. Lee, E.E. Marinero, C.J. Lin, R.F. Marks and C.J. Chien, J. Appl. Phys. **69**, 5646 (1991).

5 T. Katayama, Y. Suzuki,Y. Nishihara, T. Sugimoto and M. Hashimoto, J. Appl. Phys. **69**, 5658 (1991).

6 E. Devlin, V. Psycharis, A. Kostikas, A. Simopoulos, D. Niarchos, A. Jankowski, T. Tsakalakos, H. Wan and G. Hadjipanayis, J. Magn. Magn. Mater., in press (1993).

7 J.G. Tobin, G.D. Waddill and D.P. Pappas, Phys. Rev. Lett. **68**, 3642 (1992).

8 A.F. Jankowski, G.D. Waddill and J.G.Tobin, Bull. Amer. Phys. Soc. **38** (1), 831 (1993).

9 K.G. Tirsell and V. Karpenko, Nucl. Instrum. Meth. A **291**, 511 (1990).

10 L.J. Terminello, G.D. Waddill and J.G. Tobin, Nucl. Instrum. Meth. A **319**, 271 (1992).

11 J.L. Erskine and E.A. Stern, Phys. Rev. B **12**, 5016 (1975).

12 B.T. Thole and G. van der Laan, Phys. Rev.A **38**, 1943 (1988); B **42**, 6670 (1990).

13 B.T. Thole, P. Carra, F. Sette and G. vander Laan, Phys. Rev. Lett. **68**, 1943 (1992).

14 P. Carra, B.T. Thols, M. Altarelli and X. Wang, Phys. Rev. Lett. **70**, 694 (1993).

END

DATE FILMED

11/22/93